Simulation of intragranular plastic deformation localization in FCC polycrystals by Discrete Dislocation Dynamics

Baptiste Joste, Benoit Devincre, Riccardo Gatti, Henry Proudhon

▶ **To cite this version:**

Baptiste Joste, Benoit Devincre, Riccardo Gatti, Henry Proudhon. Simulation of intragranular plastic deformation localization in FCC polycrystals by Discrete Dislocation Dynamics. Modelling and Simulation in Materials Science and Engineering, 2023, 31 (8), pp.085021. 10.1088/1361-651X/ad02b0 . hal-04293392

HAL Id: hal-04293392
https://hal.science/hal-04293392v1

Submitted on 18 Nov 2023

HAL is a multi-disciplinary open access archive for the deposit and dissemination of scientific research documents, whether they are published or not. The documents may come from teaching and research institutions in France or abroad, or from public or private research centers.

L'archive ouverte pluridisciplinaire **HAL**, est destinée au dépôt et à la diffusion de documents scientifiques de niveau recherche, publiés ou non, émanant des établissements d'enseignement et de recherche français ou étrangers, des laboratoires publics ou privés.

Simulation of intragranular plastic deformation localization in FCC polycrystals by Discrete Dislocation Dynamics

Baptiste Joste[1,2], Benoit Devincre[2], Riccardo Gatti[2] and Henry Proudhon[1]

[1] Mines Paris, Université PSL, Centre des Matériaux (MAT), UMR7633 CNRS, 91003 Evry, France

[2] Université Paris-Saclay, ONERA, CNRS, Laboratoire d'étude des microstructures, 92322, Châtillon, France

E-mail: devincre@onera.fr

Abstract. Strain localization mechanisms taking place in polycrystal grains are investigated using Discrete Dislocation Dynamics (DDD) simulations. First, elastic Finite Element Method (FEM) simulations are used to calculate the intragranular stress distribution linked to strain incompatibilities between grains. Many configurations are tested to evaluate the stress heterogeneity and constitute a database for DDD simulations. From the analysis of these microstructures, a criterion is proposed to identify the grains where the emergence of the localization of the deformation is the most likely. Then, DDD simulations are used to explore the plastic strain localization phenomenon at the grain scale. Those simulations show that stress concentrations close to a polycrystal quadruple node can play a fundamental role in plastic strain localization. This work paves the way for future investigations to be made thanks to DDD simulations regarding slip band initiation and strain relaxation phenomena.

Keywords: Strain localization, Elastic strain incompatibilities, Dislocations, Slip bands

1. Introduction

The understanding of the deformation mechanisms of polycrystalline materials is a major challenge, especially with respect to the question of the localization of plastic deformation into slip bands and the propagation of these bands in polycrystals. In particular, many questions about the elementary mechanisms controlling these phenomena in pure metals are still open, as the way a slip band is initiated and persists in a grain. Plastic strain localization can occur for several materials, loading conditions, and temperature. Persistent Slip Bands (PSB) are a good example of plastic strain localization under particular loading conditions, i.e. cyclic loading, firstly observed by [1]. In addition, strain localization is observed at different size scales, from the nanoscale to the macroscale (in necking phenomenon for example). In order to understand and predict the macroscopic behaviour of materials, it is necessary to determine microstructural mechanisms at the origin of these phenomena.

Slip band formation as a localization mechanism has been widely observed in FCC single crystals under monotonic loading, first by optical microscopy and nowadays by electron microscopy. First observations of slip lines behaviour and kinematics have been studied by [2, 3] in Aluminium. From these results, it appears that spacing between slip bands is reduced during the deformation process as slip bands appear sporadically at first and then spread out over the observed surface. Spacing between slip bands has also been studied by [4, 5] as a function of temperature. These authors found that the spacing between slip bands increases with temperature, but also the plastic slip per band, thus promoting localization. In pure FCC polycrystalline materials, mainly copper and aluminium, slip band formation has also been studied [6, 7, 8]. As for single

crystals, slip bands are observed at the surface and in the bulk of the aggregate. The main difference between a polycrystalline structure and a single crystal is the presence of grain boundaries and the wide range of crystal orientations. The amount of plastic strain can then vary significantly from one grain to another, leading to the fact that some grains, even after large strain accumulation do not show slip bands appearing in their volume [9]. Grain interactions also complexify the understanding of slip band emergence as slip system activity inside the grain can be different depending on the closest neighbour. In addition, the interaction between a slip band and a grain boundary can lead to dislocation emission from the grain boundary on a new slip plane as expressed in [10]. As seen for single crystals, temperature, and strain rate also play a major role in slip band formation [11, 12, 13].

More recently, experimental techniques allowed to precisely measure plastic deformation and its associated mechanical fields at the subgrain scale [14, 15, 16, 17]. The main challenge of these experiments lies in the ability to perform in-situ bulk measurements, from the atomic scale to capture the features associated with dislocations, to the macroscopic scale to capture the microstructural effects. In the past few years, experimental studies have focused on the fatigue crack nucleation sites in polycrystalline Nickel-base superalloys [18, 19, 20, 21] or in other materials [22, 23] and shown the role of the microstructure in the localization of slip events. Statistical analyses under monotonic loading show the correlations between intense slip bands at the grain scale and the polycrystal microstructure [24], in particular with triple junctions location. It is well known that these triple junctions or more generally intersection zones (grain boundaries, triple junctions, and quadruple nodes) are regions where strong elastic strain incompatibility arises [25, 26]. The increase in slip band initiation probability from crystallographic features and morphology is discussed in [27], from experimental

and simulation results.

In this context and in the framework of the project *3DiPolyPlast* [28], we develop a multi-scale modeling strategy allowing a direct comparison with characterization techniques based on X-ray diffraction and electron microscopy [29, 30]. This modelling strategy is based on a coupling between FEM and DDD simulations.

In recent years, modeling of plastic strain localization using FEM has been done using crystal plasticity models (CPFEM). Such models can be fully phenomenological or more physically justified depending on the choice of the constitutive law. A detailed review of these models is given by Roters et al. [31]. Since the beginning of the 2000s, many efforts have been made to show the consistency of a crystal plasticity model, with experiments conducted on polycrystals. These comparisons have focused in particular on the ability of a crystal plasticity model to predict the plastic deformation heterogeneity, at the macroscopic and at a more local scale. First simulations were carried out on multi-crystals (a scale between the single crystal and the polycrystal, a structure classically containing 20 grains and having only one row of grains in the thickness), in the work of [32, 33], a good correspondence between macroscopic values calculated by CPFEM and experiments is obtained. With the improvement of computational capacities, crystal plasticity simulations on polycrystals have been achieved [34, 35]. More recent studies focused on plastic strain localization simulation of irradiated materials [36, 37, 38, 39] as irradiation promotes localization. Nevertheless, a precise description of plastic strain localization phenomena at the grain scale is still a difficult task. As a matter of fact, the classical FEM model depends on the spatial discretization used and on the local description of the constitutive equation. More complex models allow considering a nonlocal description, which states that the behaviour of a material point is not only dependent on its own state but also on the state of its neighbours [40, 41]. Other

models introduce characteristic length to avoid mesh dependencies and better represent physical mechanisms like plastic strain localization [42].

On the other side, since the early '90s and the first 2D simulation [43], DDD has become an essential method to describe plastic mechanisms at the mesoscopic scale. DDD simulations [44] are particularly powerful in investigating the discrete nature of plastic strain and its non-local character by modeling the individual and collective dislocation properties [45, 46]. In this context, DDD has been widely used to enrich continuous models [47, 48, 49, 50, 51] and to access precise information about dislocation microstructure evolution during plasticity. The problem of plastic strain localization has been studied through DDD simulations in alloys [52] by the mechanism of precipitate shearing, under cycle loading [53, 54] or in the case of irradiated materials [55, 56, 57], revealing the key role played by dislocation interactions on strain localization.

In the present work, mechanisms promoting incipient plastic strain localization in intense slip bands at the grain scale during monotonic tensile deformation are investigated. Pure Nickel polycrystalline aggregate is considered as a model material. The paper is organized as follows. First, the two computational methods used, i.e. the Finite Element Method (FEM) and the Discrete Dislocation Dynamics (DDD) simulation, are briefly presented. Then, the behavior of a reference grain, part of a periodic polycrystal, is studied in a linear elastic framework using FEM in a systematic way according to the aggregate microstructure (orientations and shapes of grains). With this we will highlight the effect of elastic strain incompatibility, trying to better understand the origin of the heterogeneity of intragranular stress and strain fields. In addition, a criterion to identify within an aggregate the most favorable grain for plastic strain localization is proposed. This criterion is proposed on the basis of FEM calculations, which means that statistical trends can be obtained with much

shorter calculation times than with the DDD. Lastly, DDD simulations are performed to elucidate the role of elastic strain incompatibilities on dislocation microstructure evolution. The outcome of these simulations highlights more intense slip activity, even at low total plastic strain, in the regions with larger stress concentrations.

2. Computational methods

As introduced in the previous section, we propose to study the problem of intragranular plastic strain localization through two simulation methods, FEM and DDD. It is commonly accepted that these two simulation methods are complementary since FEM provides a good description of the complex boundary conditions of a polycrystalline aggregate and DDD offers a more justified description of plastic mechanisms. In addition, FEM allows computing the polycrystalline behaviour of representative aggregates (with several grains) [58, 59, 35] whereas DDD simulations are more limited to the modelling of one or few grains due to limits in computational capacities. In this work, to take advantage of both methods, a weak coupling between FEM and DDD is proposed. FEM computations will be used to model the behaviour of all grains in the aggregate during the elastic part of the loading, thus providing necessary boundary conditions for the DDD computation. One grain of the aggregate is then selected to run DDD simulations to model its plastic behaviour. A detailed description of simulation parameters and main characteristics is given in subsection 2.1 and subsection 2.2.

2.1. FEM simulations

Finite Element simulations were run using the *Z-set* software package jointly developed by Ecole des Mines de Paris and Onera [60]. Polycrystalline aggregates have been generated and meshed with c3d10 elements by the open source software *Neper* [61],

well suited for building up Voronoi and Laguerrre tessellations. In order to explore the intragranular elastic behaviour in a systematic way, three distinct series of simulations of polycrystalline aggregates were performed. The first series of simulations (series 1) considers a change in the crystalline orientation of neighbouring grains relative to a reference grain chosen in the aggregate. For this reference grain, the crystalline orientation remains unchanged for all simulations. Referring to the notations in figure 1, this means changing the neighbouring grains' matrices $\boldsymbol{P}_j$ while the grain orientation matrix $\boldsymbol{P}_i$ is fixed. The second series of simulations (series 2) consider the modification of the reference grain crystalline orientation while orientations of its neighbouring grains are fixed. Again referring to figure 1, this means changing the grain orientation matrix $\boldsymbol{P}_i$ while the other orientation matrices $\boldsymbol{P}_j$ are fixed. Finally, the third series of simulations (series 3) is used to study the role of the morphology (grain size, aspect ratio) while the reference grain crystalline orientation is fixed. Series 1 and 2 contains two hundred draws, while series 3 contains only one hundred draws. In each series, quantities of interest like heterogeneity, stresses, and strains are computed.

Simulation parameters are also listed in table 1 and are identical for every five hundred simulations. Elastic constants for pure nickel can be found in [62]. The aggregates constructed are elementary periodic units that can be repeated ad infinitum, so the boundary conditions used are periodic boundary conditions, allowing us to avoid boundary effects. At each Gauss point, the resolved shear stress is computed for each slip system s thanks to the Schmid law :

$$\tau^s = \boldsymbol{\sigma} : \mathbf{m}^s \tag{1}$$

With $\boldsymbol{\sigma}$ the Cauchy stress tensor and $\boldsymbol{m}^s$ the orientation tensor defined as :

$$\mathbf{m}^s = \frac{1}{2}(\underline{n}^s \otimes \underline{l}^s + \underline{l}^s \otimes \underline{n}^s) \tag{2}$$

let us note $\underline{n}^s$ the normal to the slip plane and $\underline{l}^s$ the slip direction.

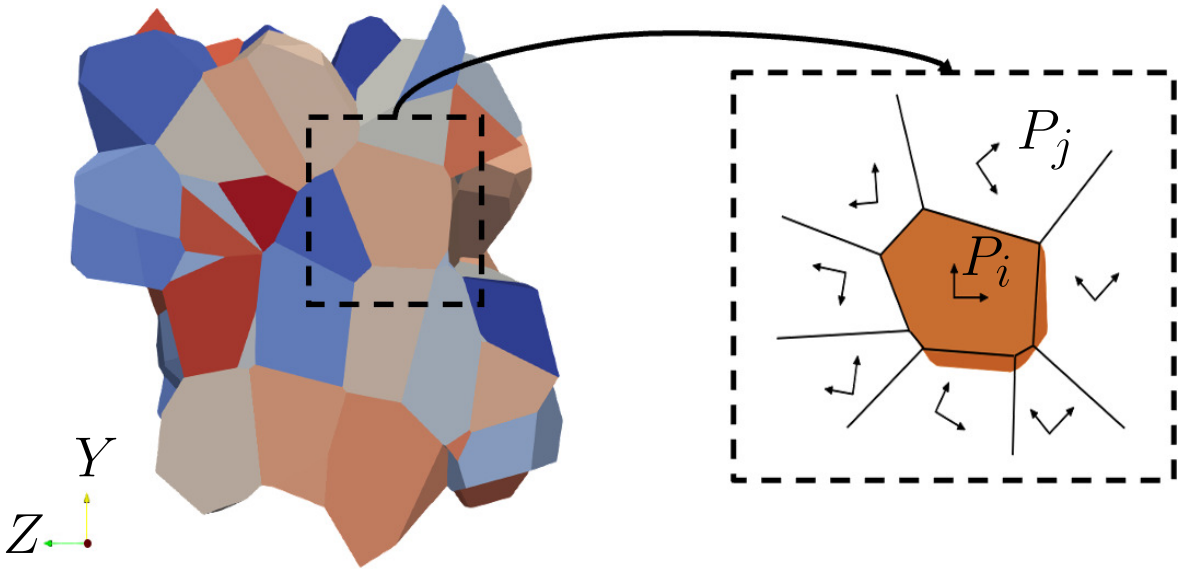

Figure 1: Schematic of the simulations associated with series 1 and 2 used in the present work. On the left side is the reference periodic aggregate used in series 1 and 2. On the right side, the definition of $\boldsymbol{P}_i$ and $\boldsymbol{P}_j$, the orientation matrix of the reference grain (in orange) and the orientation matrices of the neighboring grains, respectively. In the first simulations series, the orientations of $\boldsymbol{P}_j$ while keeping $\boldsymbol{P}_i$ constant are randomly changed. In the second simulations series, the orientation of $\boldsymbol{P}_i$ while keeping $\boldsymbol{P}_j$ constant is randomly changed. Lastly, in the third simulations series, one hundred aggregates with different grain morphologies are randomly defined while keeping the reference grain orientation constant.

Table 1: Simulation parameters for the FEM computations presented in this article.

Aggregate size (μm)	**Anisotropy coef.**	**Mean grain size (μm)**
95 $\times$ 95 $\times$ 95	2.51	24
$\boldsymbol{C_{11}}$ **(GPa)**	$\boldsymbol{C_{12}}$ **(GPa)**	$\boldsymbol{C_{44}}$ **(GPa)**
246.5	147.3	124.7
Burgers vector (m)	**Loading**	**Series 1†**
2.489×10^{-10}	$\langle E_{zz} \rangle = 0.1\%$	$\dot{\boldsymbol{P}}_i = 0$, $\dot{\boldsymbol{P}}_j \neq 0$
Series 2†	**Series 3***	**Draws per series**
$\dot{\boldsymbol{P}}_i \neq 0$, $\dot{\boldsymbol{P}}_j = 0$	Morphology	200(†)/100(*)

To the best of the author's knowledge, a systematic analysis of the role of the microstructure on the intragranular elastic loading has never been reported, especially considering local values. Few authors have studied the polycrystalline elastic behaviour statistically but focused on average stress values variation and not with the scope of plastic strain localization phenomena [63, 64, 65].

2.2. DDD simulations

DDD simulations were run with the 'microMegas' code [66] and using a kind-like superposition principle [67, 68] as already discussed. This solution is preferred to other methods like the discrete continuous model [69, 70] for reasons of simplicity. The heterogeneous stress applied inside the simulated grains ($\boldsymbol{\sigma}_{FEM}$) is the sum of a mechanical loading corresponding to the tensile test in the Z direction (see table 1) and the stress field induced by the incompatibility of elastic deformation between the grains, part of the polycrystalline aggregate. The stress field $\boldsymbol{\sigma}_{app}$ is calculated directly with the FEM simulations presented in subsection 2.1. The simulated grain in DDD is supposed to be surrounded by fully linear elastic grains, this hypothesis allows for faster computations as the initial $\boldsymbol{\sigma}_{FEM}$ can be updated by applying a pre-factor. This process is further described later in this section. Such a hypothesis is supposed to be valid as the total plastic deformation calculated during DDD simulations is small (less than 0.001). In addition, the simulated grain is supposed to be the first one to trigger plasticity in the aggregate, this point is better detailed in subsection 3.3.

The initial microstructure is made of a random distribution of Frank-Read sources. That kind of initial microstructure is known to describe well the plastic behaviour of large grains in DDD simulations [71]. The reason the use of Frank-Read sources is preferred in this work is motivated by the desire to consider low dislocation density in the initial configurations. Indeed, the dislocation density is increasing very fast in such

simulations, and for numerical reasons, it is useful to start the computations with a low number of dislocation sources. With low dislocation density, if one uses configurations made of relaxed loops, the number of junctions anchoring the dislocation network is low and may not be sufficient to stabilize the few dislocation sources in the volume of the grain. This well-known problem is even amplified in this work focusing on the plasticity of polycrystals. In such types of materials, the flow stress is high enough to result in the destruction of all the formed junctions during the relaxation process. Frank-Read sources are described by their length, their character, and the fact that they are pinned at both ends by infinitely rigid pinning points [72]. For our simulations, we impose initial dislocation segments of length 5 μm, the initial dislocation density is $\rho^s_{ini} = 1 \times 10^{11}$ m^{-2}, which correspond to a set of 30 Franck-Read sources per slip systems and the grain boundaries facets are impenetrable barriers for dislocations. All simulations are made at a constant plastic strain rate $\dot{\varepsilon}^p_{zz}$ equal to 200 s^{-1}.

To impose a constant plastic strain rate, a proportionality coefficient, $0 < \alpha < 1$, is applied to the elastic stress field solution calculated with the FEM simulations of the subsection 2.1 at 0.001 total deformation. Such a solution has already been used in [73] to model size effects in nanoparticles. Thus, let's note :

$$\boldsymbol{\sigma}_{app} = \alpha \times \boldsymbol{\sigma}_{FEM} \tag{3}$$

with the proportionality coefficient α computed at any time step t from the relationship :

$$\alpha_{t+\Delta t} = \alpha_t + \Delta\alpha \tag{4}$$

and,

$$\Delta\alpha = \frac{(\dot{\varepsilon}^p - \dot{\varepsilon}^p_m) \times \delta t}{\zeta} \tag{5}$$

where $\dot{\varepsilon}^p$ is the desired plastic strain rate, $\dot{\varepsilon}^p_m$ is the measured plastic strain rate at the time δt and in a given direction, ζ is a scaling factor.

To calculate the local intragranular plastic strain field, a specific post-processing is used. A discretization of the grain into voxels is performed which allows the calculation of the area swept by each dislocation segment, ∂S^i, due to the motion of dislocation lines in each voxel of volume V. These swept areas are directly related to the elementary plastic strain associated with each slip system, ∂S^i, as :

$$\partial \gamma^i = \frac{b_i \times \partial S^i}{V} \tag{6}$$

This provides a precise measure of slip system activity inside the grain at the scale of a few slip plane spacing. One example is illustrated in figure 2-(b) where the activity of $(\overline{1}11)$ slip planes can easily be identified. Applying various visualization thresholds allows us to only visualize the most intense slip events and then quantify slip localization events during the simulations. On the other hand, figure 2-(a) offers a more global description of the slip system activities, following the evolution of the average plastic slip as a function of the average applied stress inside a grain.

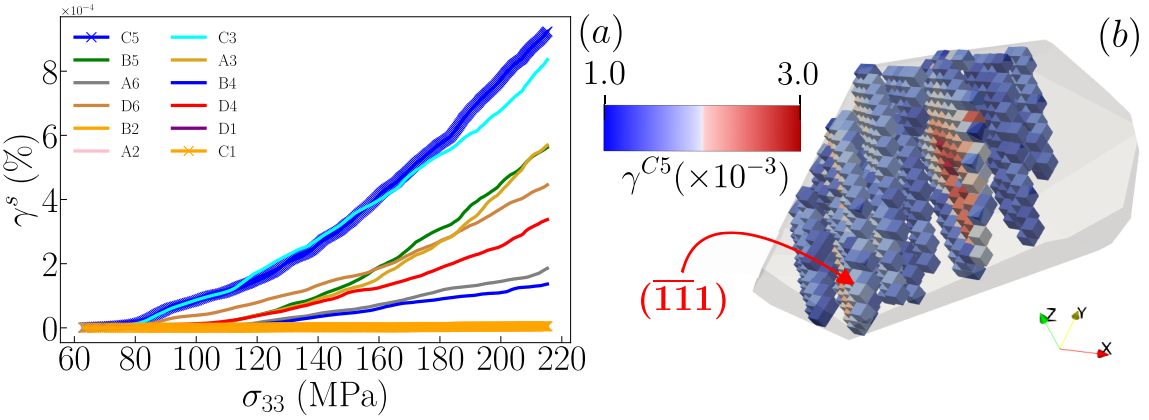

Figure 2: Heterogeneity of the plastic deformation inside the grain. (a) Illustration of the slip system activity on the whole grain as a function of the increasing applied stress. (b) Visualization of slip system activity of slip system $C5$ for $\gamma^{C5} \in [1. \times 10^{-3}; 1.7 \times 10^{-3}]$ whose average mesoscopic value is $\langle \gamma^{C5} \rangle = 0.6 \times 10^{-3}$.

3. Investigation of the elastic properties

As observed in the literature, the intragranular elastic loading is supposed to play an important role in plastic strain localization, as most intense slip bands looks to be influenced by the so-called intersection zones [24]. Therefore, the detection of elastic strain incompatibility between the grains is important as it is the source of the strain and stress field heterogeneity inside the grains. In this section, FEM calculations are used to investigate this effect. The reference grain is randomly selected from the microstructure used in series 1 and 2, then reused for series 3.

Figure 3 shows the dispersion of the local resolved shear stress inside the reference grain for a given set of orientations. Histograms show values computed at each Gauss point of the defined mesh (the whole mesh contains 1843230 Gauss points and the reference grain contains 11890 Gauss points). Significant dispersion of resolved shear stress values can be observed by the amplitude $\Delta\tau^s = |\tau^s_{max} - \tau^s_{min}|$ as the average dispersion of all slip systems is approximately ± 30 MPa from the mean resolved shear stress value computed over the total grain volume. This behaviour is very different from that of single crystals, as dispersion is the direct result of incompatibility in elastic deformation. Looking at $\Delta\tau^s$ values, not many differences are reported from the comparison between slip systems, although Schmid factors are very different (see table 2). This first result therefore shows that the calculated stress dispersion is influenced more by interactions with neighbouring grains than by the grain's own orientation, once again highlighting the predominant role of elastic deformation incompatibility.

A complementary observation of the resolved shear stress field dispersion is provided by figure 4 showing a mapping of the resolved shear stress at the surface of the reference grain with two different visualization viewpoints (a) and (b). Computation of the

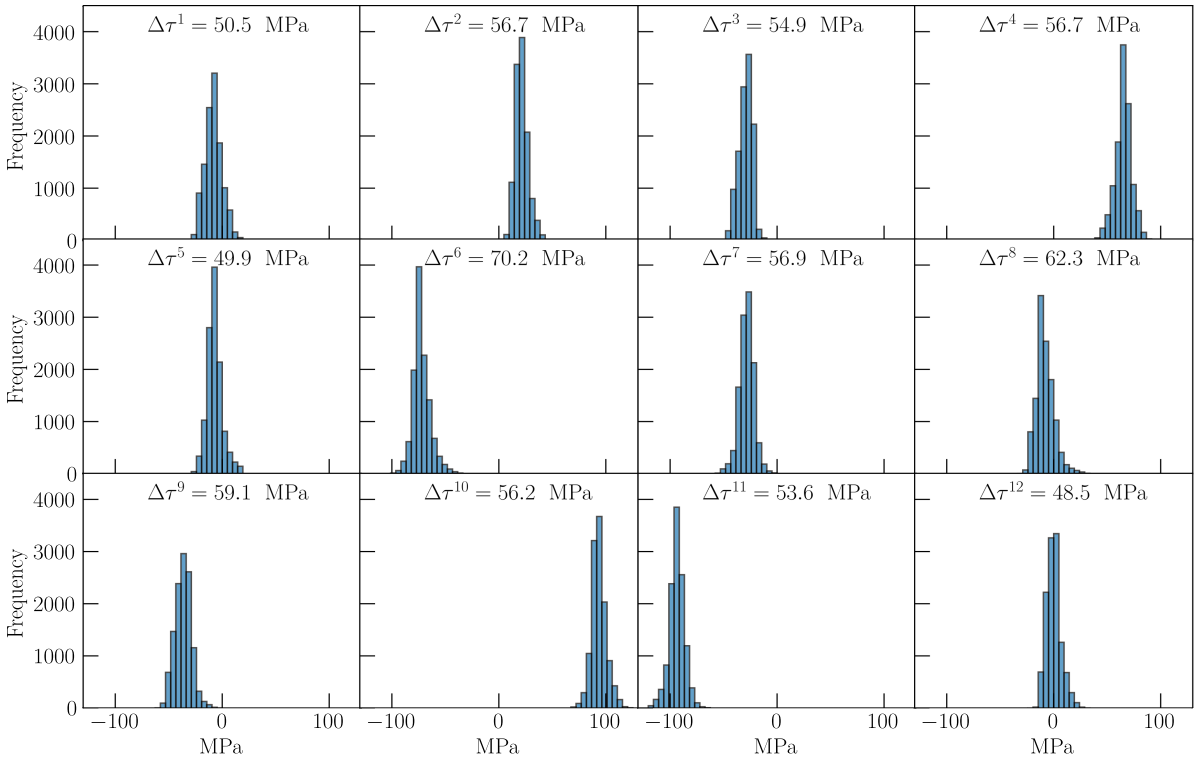

Figure 3: Distributions of the resolved shear stress τ^s computed at each Gauss point inside the reference grain for one of series 1 simulations on the twelve FCC slip systems (from 1 to 12).

resolved shear stress is made on the most active slip system C5. The field is strongly heterogeneous at the surface of the grain and zones of lower or higher intensity are mainly located near intersection zones. These dispersion regions are quite thick (∼10 μm) and can be amplified by increasing the stiffness differences between the grains in contact. Similar results are given in [27] where strain field dispersion is found to be mostly influenced by the anisotropy ratio A.

This first set of calculations shows the importance of statistically analyzing the elastic interactions between grains. More details and an analysis of the role of the aggregate microstructure on intragranular elastic loading are given in the next subsection.

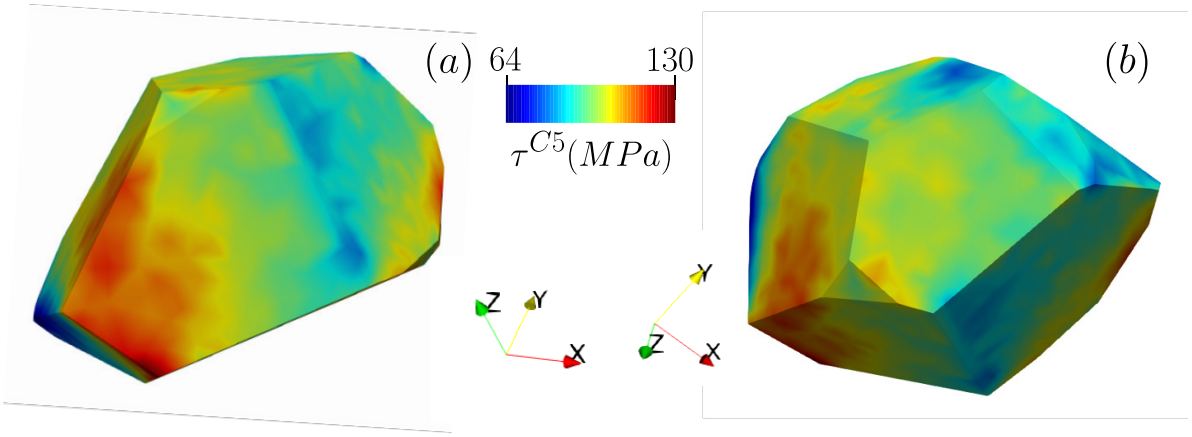

Figure 4: Shear stress mapping resolved at 0.1% strain, (a) the reference view of the DDD-simulated grain that will be used in the following, and (b) an alternative view. Stress values are extrapolated to the nodes.

3.1. Statistical analysis of the aggregate microstructure effect

Following the protocol described in subsection 2.1, a total of five hundred different aggregate configurations are created. We first analyze the results of series 1 (configurations where the orientation of a reference grain is constant while the orientations of all the other grains are modified at each run), which will be compared with series 2 and 3 later. Analysis of the Schmid factor values reveals two predominant slip systems, C5 and C3, which are coplanar, and two other slip systems with relatively high factors, D4 and D6.

As shown in figure 3, elastic strain incompatibility appears to play a major role in the stress distribution within the grain. Since the shear stress deviations resolved on each slip system do not vary much from one slip system to another, it should also be noted that the Schmid factor has little or no influence on the amplitude of the stress heterogeneity.

To study the role of the neighboring grains on the average intragranular resolved shear stress, the orientation of all other grains is now randomly modified for each computation. Figure 5 shows for two hundred draws, the distribution of the average

Table 2: Solution of the calculation of the theoretical unidirectional Schmid factors with a theoretical tension along Z-axis and for the 12 FCC slip systems in the reference grain 'i' of the series 1. The latter orientation is given according to the Euler angle convention $(\phi_1, \Phi, \phi_2) = (27.790, 48.067, 167.920)$, in degrees. Schmid-Boas notation is used to index slip systems.

Slip System	**1-B4**	**2-B2**	**3-B5**	**4-D4**
Schmid factor	0.02	0.05	0.03	0.325
Slip System	**5-D1**	**6-D6**	**7-A2**	**8-A6**
Schmid factor	0.03	0.362	0.122	0.05
Slip System	**9-A3**	**10-C5**	**11-C3**	**12-C1**
Schmid factor	0.07	**0.447**	0.417	0.03

intragranular resolved shear stress on each slip system in the reference grain with 11890 Gauss points. We first notice from this figure that the slip system hierarchy as planned by the Schmid factors is globally respected for all the orientation sets. Slip systems C5 and C3 have the most intense resolved shear stress followed by D4 and D6. Nevertheless, the aggregate microstructure strongly influences the average resolved shear stress intensity as highlighted by the comparison with the Schmid factors prediction (dotted vertical lines). Those values are computed considering the grain as a single crystal, thus not taking into account elastic strain incompatibility. In some cases, the effect of the surrounding microstructure on the reference grain leads to an increase (slip system 3) or a decrease (slip system 10) in the average resolved shear stress with respect to considering the grain as a single crystal. These variations can be important, an average standard deviation of 5 MPa is computed on every slip system. Thus, without changing the orientation of the reference grain, the intragranular elastic load depends on interactions with neighboring grains, but the hierarchy of the slip system's activity remains unchanged.

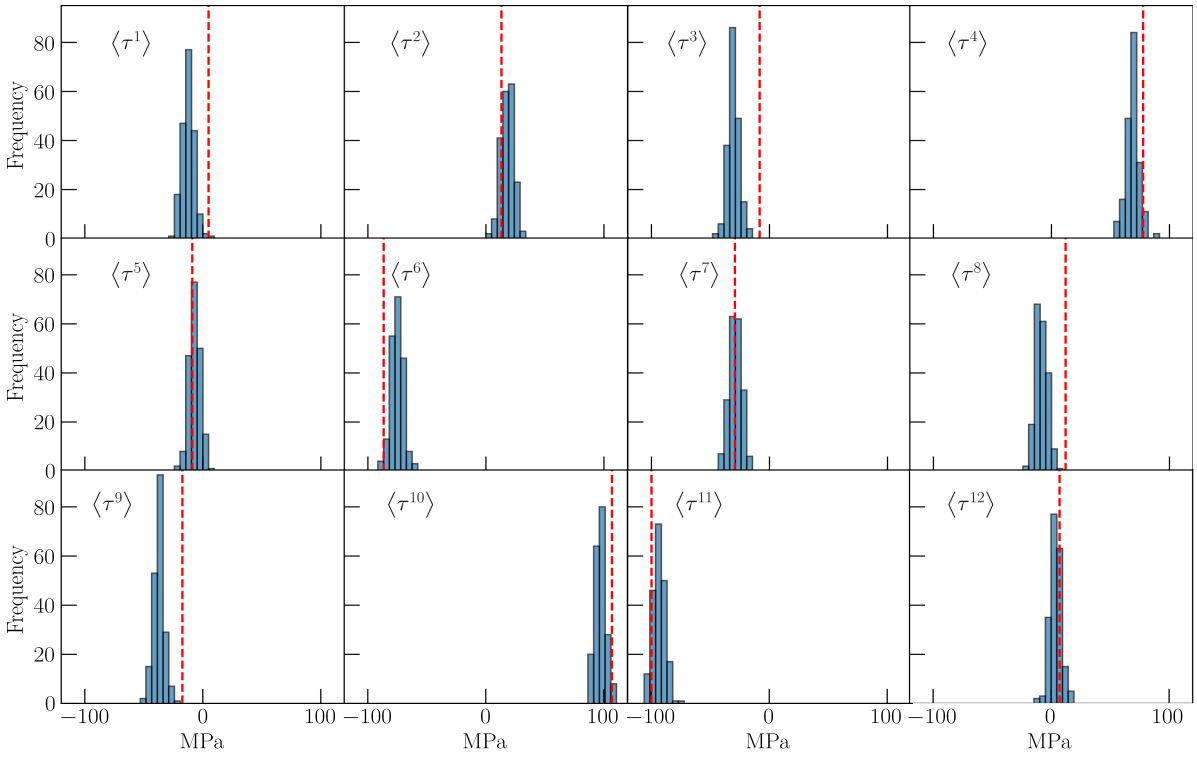

Figure 5: Histograms of the mean resolved shear stress $\langle\tau^s\rangle$ for all slip systems (from 1 to 12) on the reference grain 'i' for the 200 configurations randomly drawn of series 1. The dotted lines represent the single crystal prediction for the homogeneous stress solution.

Keeping in mind the fact that anisotropy clearly influences the stress and strain field dispersion, it is of major interest to quantify the intragranular heterogeneity for all the configurations. There, we propose to describe the heterogeneity of a mechanical field by its standard deviation following the relation: $\sqrt{V_a^s} = \sqrt{\frac{1}{n}\sum_{i=1}^{n}(\tau_i^s - \overline{\tau_i^s})^2}$. This is computed for all the configurations and for all slip systems and reported in figure 6. The use of the amplitude as in figure 3 to quantify heterogeneity is not advised, as in elasticity no convergence from the mesh size can be obtained on the maximum or minimum resolved shear stress values near grain boundaries. Standard deviation is well more suited to give a justified quantification of heterogeneity and in our computations, a convergence is quickly reached when increasing the mesh density.

Once again, and in accordance with the results of figure 6, the Schmid factor seems

to play a minor role as the shape of the histograms is more or less the same for all the slip systems. In addition, the mean standard deviation calculated for each slip system shows very similar values. The dominant factor seems to be the interaction between the grains because from one configuration to another, on a particular slip system, the standard deviation can vary greatly. For example, heterogeneity can vary from 5 MPa to 13 MPa in the same grain for two different configurations.

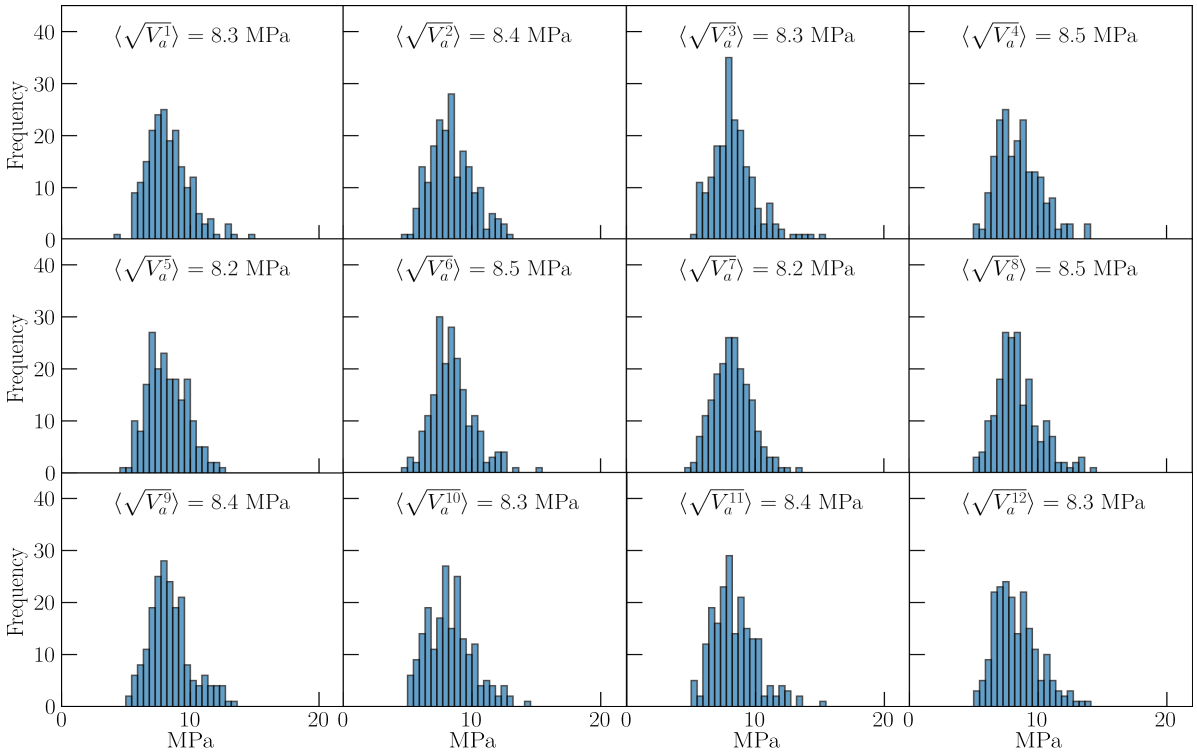

Figure 6: Standard deviation calculated on each slip system (from 1 to 12) on the reference grain and for each configuration of the series 1 simulations.

Figure 7 illustrates this difference in the case of a low or high standard deviation. Here, we see that the highest resolved shear stress in the grain is increased by 50 MPa from one configuration to another. However, the average resolved shear stress in both configurations remains the same, meaning that the increases between the lower and upper stress areas balance out.

The above results demonstrate the important role of elastic interaction between

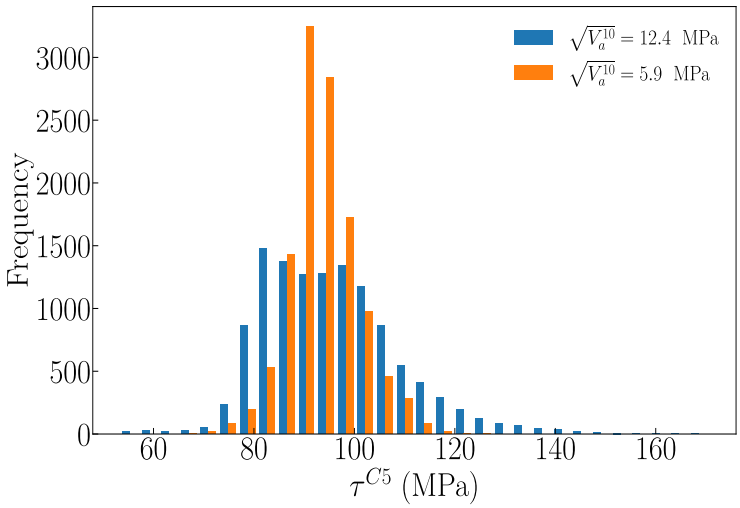

Figure 7: Illustration of the resolved shear stresses for two different configurations of neighbours grain orientations which correspond to the case of a low or high standard deviation. Slip system C5 distribution is represented.

neighboring grains leading to elastic strain incompatibilities that modify the intragranular elastic loading of the reference grain. On the one hand, the orientation of the reference grain well defines the hierarchy of the slip systems that will be mainly active, on the other hand, the orientation of the neighboring grains seems to be the most important parameter to determine the amplitudes and heterogeneity of the intragranular loading stress controlling the dislocation dynamics.

Equivalent observations are made for series 2, where the orientation of the reference grain is modified while other orientations are kept constant. From the results of series 2, changing the reference grain orientation also leads to important modification of the intragranular elastic loading. As the orientation is modified for every configuration, one should refer to the standard deviation computation to better interpret the effect on the intragranular elastic loading. In figure 8, series 1 and 2 are compared highlighting some differences. On this figure, the cumulative frequency ($f_n^{cum} = \sum_{i=1}^{n} f_i$) is computed to highlight differences between both series. It is observed that a quasi-systematic shift in

the standard deviation values appears between the two series. Indeed, every slip system, except for slip system 5, shows in the reference grain a more intense standard deviation (more heterogeneous patterns) in the case of the series 1 simulations.

From the second set of simulations (series 2), we can conclude that the exploration of heterogeneity within grains is simpler using the simulation protocol of series 1 simulations, which allows modelling larger amplitudes of heterogeneity. Changing the orientation of the grains surrounding a reference volume fixed within an aggregate is therefore the simplest approach to a systematic numerical exploration with DDD simulations.

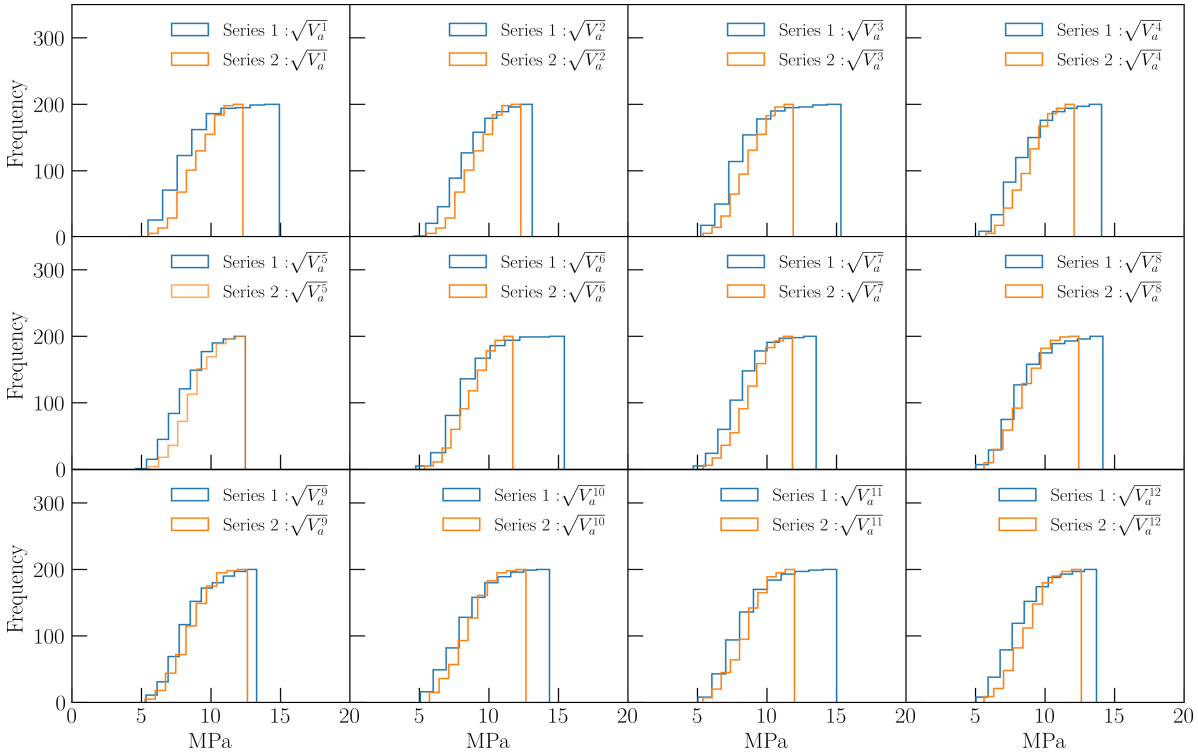

Figure 8: Comparison of the calculated standard deviation of the intragranular stress for both simulations series 1 and 2, values are represented as a function of the cumulative frequency for all the slip systems (from 1 to 12).

The last series of simulations (series 3) we tested to better understand and control elastic heterogeneity in a periodic aggregate is now briefly presented. This series of simulations is based on a variation of the morphology of the grains such as their diameter

and aspect ratio. In these simulations, a reference grain is selected and the size of neighbouring grains vary randomly, but the set of grains must always form a periodic aggregate and the total volume of the simulation must be the same.

This series 3 leads to the same results as those observed in series 1 and 2, but with smaller heterogeneity amplitudes as illustrated in figure 9-(a) in comparison with "Series 1", "Series 1, set 2" and "Series 1, set 4" curves. The "Series 1, set 2" curve and "Series 1, set 4" curve (green and purple curves in the figure) represents the evolution of the average standard deviation on all slip systems for two other crystalline orientation of the same reference grain:

(i) $(\phi_1, \Phi, \phi_2) = (287.801, 101.222, 16.740)$

(ii) $(\phi_1, \Phi, \phi_2) = (16.797, 75.154, 271.874)$

The curves of "Series 1", "Series 1, set 2" and "Series 1, set 4" show close evolution highlighting a weak dependency from the crystalline orientation. In comparison, in series 3 simulations, the number of grains in contact with a reference grain is often modified and generally reduced as seen in figure 9-(b). For the hundred build configurations, only 8% of them have a number of neighbours equivalent to or higher than the one in series 1 and 2. This result strongly suggests that there is a correlation between the number of neighbours and heterogeneity. Close attention to the "Series 1, set 3" curve consolidates this assumption. Indeed, this set of calculations is realized considering a reference grain with a lower number of neighbours, 12 in total (against 23 for "Series 1", "Series 1, set 2" and "Series 1, set 4"), but with the same crystalline orientation as for the "Series 1" curve. The average standard deviation calculated for this series of simulations is lower due to the smaller number of neighbours. What these results demonstrate is that intragranular elastic loading heterogeneity is statistically amplified with a high number of neighbours. Indeed, the larger this number, the larger the probability of being in

contact with much "harder" or much "softer" grains.

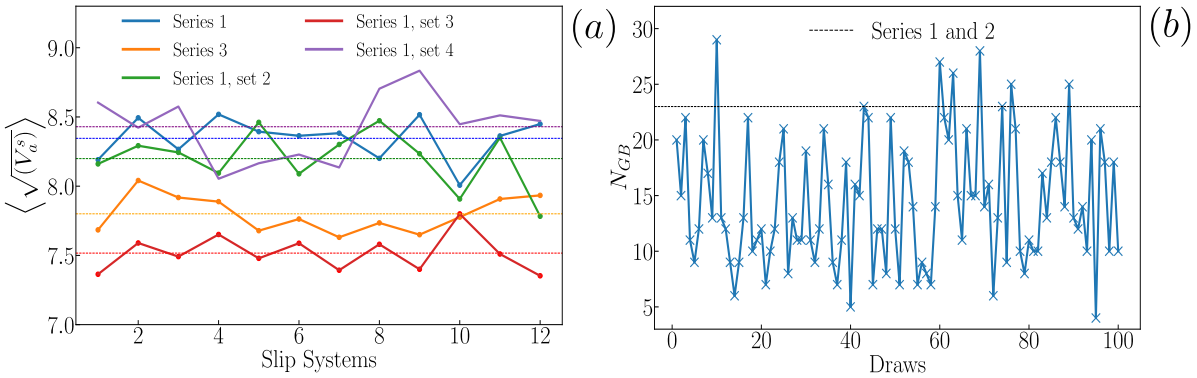

Figure 9: Comparison of the average standard deviation per slip system between series 3 and various sets of series 1 (a). Sets 2 and 4 correspond to the series 1 statistical analysis with two other crystalline orientations of the reference grain while set 3 corresponds to the series 1 statistical analysis with a reduced number of neighbours. The number of neighbours is represented by the number of grain boundaries N_{GB} for the reference grain and for every configuration in series 3 (b). As a comparison, the dashed line represents the number of neighbours for series 1 and 2 simulations (23 neighbours).

3.2. Stress concentration analysis

The numerous observations from the three series studied in section 3.1 (see for instance the results in figure 4) and from the literature show that the heterogeneity of the stress field is not constrained to isolated points, but refers to more mesoscopic regions with length comparable with the grain size. These regions are located near intersections in between grains as grain boundaries, triple junctions, and quadruple nodes. One way to validate these observations from our statistical analysis is to plot the evolution of the resolved shear stress on a particular slip system as a function of the distance to the quadruple node (see figure 10). In our simulations, quadruple nodes are supposed to be the most critical intersection for the emergence of stress concentration leading to heterogeneity as it represents the intersection among the largest number of grains.

Figure 10-(a) shows the evolution of the resolved shear stress in the reference grain volume as a function of distance to the N quadruple node existing on the surface of the

grain (in series 1). The calculation is performed as follows: for each configuration, the stress concentration regions are identified by calculating the maximum resolved shear stress on the mesh. Then, from these regions, the distance to all N quadruple nodes is calculated and the smallest one is selected. As a result of all these computations, an average curve is plotted as in figure 10-(a) representing the average evolution obtained from all the configurations. It should be noted that quadruple nodes are also the regions where low stresses can be concentrated depending on the neighbouring grains' configuration. Figure 10-(a) confirms that stress concentration regions are systematically observed in the vicinity of quadruple nodes and the way the stress decreases from the quadruple nodes, progressively, shows that the stress concentration is more or less distributed in the vicinity of the quadruple nodes.

Another interesting observation is that the calculated stress in those specific regions decreases at the center of the grain to values close to the grain mean value. Hence maximum and minimum stress regions are more expected close to the grain boundaries. The figure 10-(b) shows an example of one specific configuration with a stress concentration near one quadruple node and three triple junctions, this region is spread at the grain surface (about 10 μm long). It is hard to quantify if stress concentration regions are systematically of this importance (in terms of stress intensity and spatial distribution) but it has been observed in many configurations tested in the present work.

Besides reported computations, many attempts have been made to identify a simple mathematical model to predict the emergence of stress concentration within grain from its own configuration and the one of its neighbours. Such research appeared to be difficult as the number of neighbours can be large (see figure 9-(b)) for a given grain, resulting in many possible configurations. The simulation results strongly suggest that

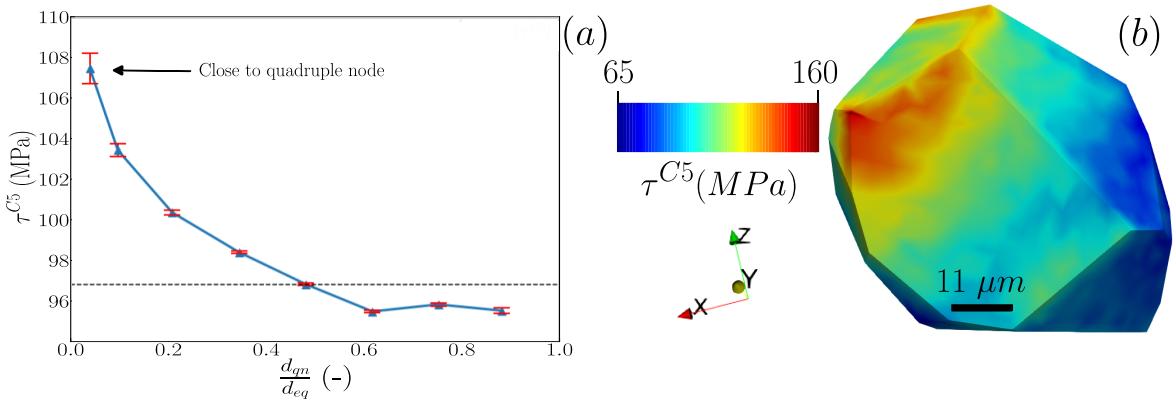

Figure 10: Illustration of the existence of stress concentration near quadruple nodes. (a) Variation of the resolved shear stress τ^{C5} as a function of distance from the quadruple nodes d_{qn} divided by grain diameter d_{eq}. This curve is computed from all configurations of the simulations series 1. The dashed line represents the mean resolved shear stress computed in the full grain volume $\langle \tau^{C5} \rangle$. (b) Visualization of the stress gradient for one particular configuration where stress concentration zone is observed close to one quadruple node.

the primary parameter explaining the presence of stress concentration and heterogeneity in an aggregate is the disorientation between neighboring grains. Nevertheless, no simple relationship has been found based on a direct calculation of the disorientation between grains in contact. Alternatively, we explored other possibilities like focusing our study on grain triplets. We define grain triplets as three grains in contact with each other and with the reference grain, thus defining a quadruple node intersection. In this case, we focused on computing the strain dispersion in the triplets, also leading to very low correlation coefficients. What these attempts suggest is that the problem of stress fluctuation within a grain is a very local problem depending on every interaction and cannot be assimilated to a less local variable that would suppose interactions to be averaged.

3.3. Identification of the most favorable grains for a localization of the plastic deformation

On the basis of the previous results and observations, we have proposed a simplistic criterion based on elasticity, which makes it possible to select, within a simulated aggregate, the grains that are expected to plastically deform first and that exhibit a high degree of stress heterogeneity, i.e., the grains most favorable to the observation of strong localization of the early stages of plastic deformation.

This criterion is based on the correlation between two quantities, the intensity of the resolved shear stress and the level of heterogeneity, as shown in figure 11. The use of quantities projected onto slip systems as resolved shear stresses instead of stress tensor components or invariants is justified by our will to study plastic strain localization at the scale of dislocations. The first grain to plastify is expected to be the one with the most intense resolved shear stresses and the most heterogeneous field. As a matter of fact, in equation 7 we define an average over all the slip systems of the resolved shear stress maximum values calculated at Gauss points, and in equation 8 an average on slip systems of the standard deviation value ($\sqrt{V_a^s}$). To give more weight to the most active slip systems in this criterion, we add to the computation of the standard deviation a correction by the Schmid factors (m^s). In addition, the calculation result is weighted by the average Schmid factor ($\langle m^s \rangle$), which represents the expected average plastic activity for the given crystalline orientation. This normalizes the results and makes them independent of the number of active slip systems.

$$\langle \max(\tau^s) \rangle = \frac{\sum_{s=1}^{12} \max(\tau^s)}{12} \tag{7}$$

$$\Lambda = \frac{\sum_{s=1}^{12} \sqrt{V_a^s}}{12} \times \frac{m^s}{\langle m^s \rangle} \tag{8}$$

Figure 11 presents the evolution the corrected standard deviation Λ as a function of

maximum resolved shear stress $\langle \max(\tau^s) \rangle$ for three distinct following simulation cases:

a) a test performed on one aggregate containing a hundred grains;

b) a test performed on a grain for which we modify the orientation a hundred times;

c) a test performed on two grains of different orientation for which neighbours orientations are changed a hundred time.

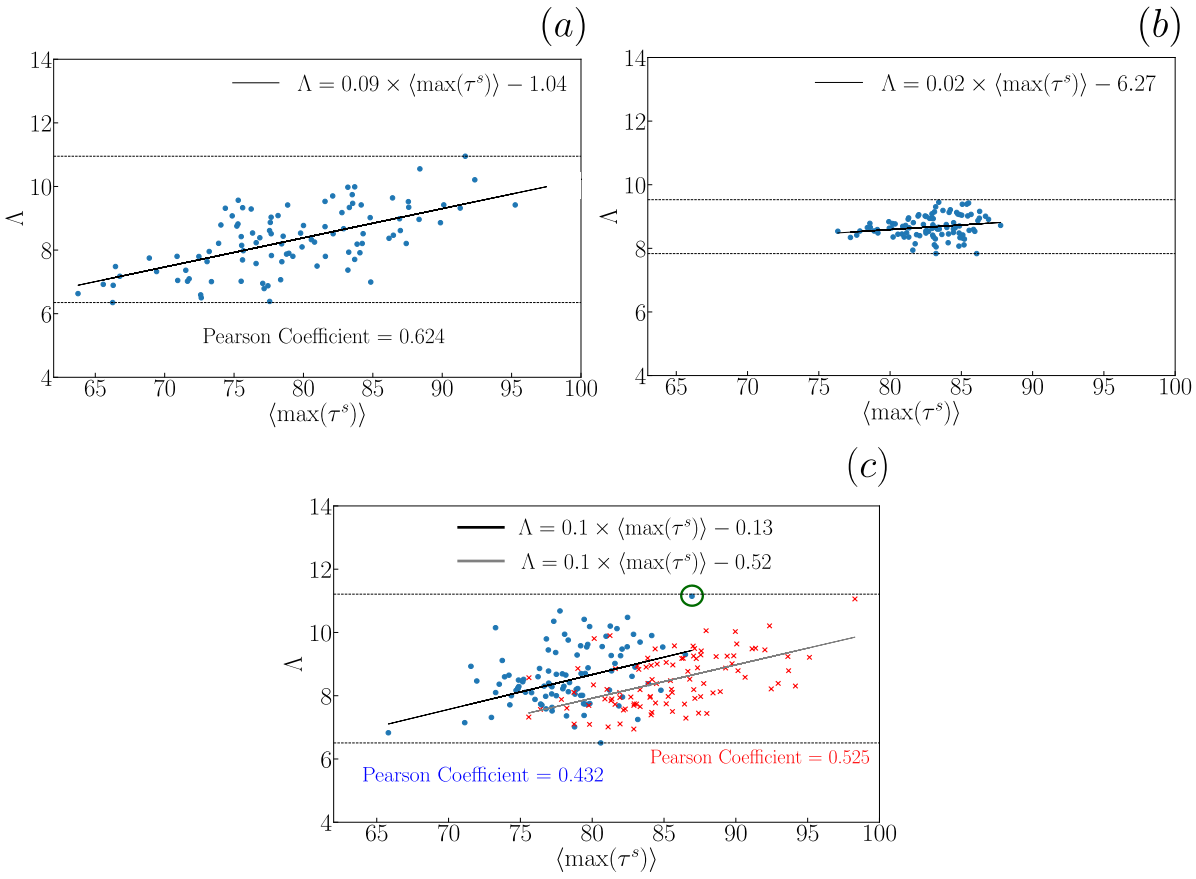

Figure 11: Corrected standard deviation Λ evolution as a function of maximum resolved shear stress $\langle max(\tau^s) \rangle$ for three different cases explained in the text. Horizontal lines represent the maximum and minimum values of the interval. The criterion is applied to a random aggregate (a), to a grain whose orientation varies (b) and to two grains of different orientations for which neighbours orientations are changed (c). The green dot shows the configuration used in section 4.

By applying the formulations presented in equation 7 and equation 8, it is possible to classify the configurations (grains or orientations) from the most favourable to the

appearance of localized plastic deformation to the least favourable. For each of the examples, a linear regression is calculated from the point clouds derived from the statistical data. In graphs (a) and (c), the slopes calculated are almost identical, showing that the criterion is consistent. The Pearson coefficients [74] calculated on these two graphs indicate a good correlation and justify the link between the presence of stress concentration and the presence of intragranular heterogeneity. The two trends presented in graph (c) show an equivalent slope, the two linear regression curves are parallel but have a slightly different Pearson coefficient certainly linked to the number of points used for the statistics. If we look a little more closely at the evolution shown in graph (b), we can see that the slope calculated is weaker. Furthermore, the correlation coefficient calculated for this case study is very low and does not allow us to conclude on the presence of a correlation. In addition, we can see that for this particular case, the corrected standard deviation and maximum resolved stress value intervals are small. This last statement reflects the greater difficulty in obtaining heterogeneous configurations within the framework of series 2 simulations, as illustrated in figure 8, and demonstrates once again the importance of the neighbourhood in comparison with reference grain crystalline orientation.

This simple relationship between heterogeneity and resolved shear stress concentration was developed for the present study in order to identify the most important grains in simulated aggregates on which data analysis with DDD simulations can be focused. We note in passing that this criterion can also be used to help identify the grains to be monitored as a priority during in situ experiments.

4. Investigation of the plastic behaviour

4.1. Plasticity and elastic strain incompatibilities

It is now clear that elastic strain incompatibilities between grains play a major role in intragranular elastic loading. To see how plastic deformation is affected by stress heterogeneity within the grain, DDD simulations are performed on a configuration of interest selected from the simulations series 1 (see figure 11-(c)).

DDD simulation conditions are the following: Plastic slip is considered on the twelve slip systems of the FCC structure. We first decided to run simulations without considering the possibility of dislocation to cross-slip. The resolved shear stress dispersion associated with the simulated configuration is reported in figure 7. To avoid biases coming from initial conditions, the plastic strain is averaged with the results of 5 simulations started with different random dislocation source configurations :

$$\gamma_{av}^{C5} = \frac{1}{5} \times \sum_{k=1}^{5} \gamma_{k}^{C5} \tag{9}$$

All the other important simulation parameters are described in section 2.2.

Figure 12 shows the results of the most intense slip traces observed during the simulations (a) and the intragranular elastic loading associated with the chosen configuration (b). We can compare the location of the simulated slip traces with the applied stress field and see that the most intense slip trace develops near a region of stress concentration.

Note that this result is obtained without cross-slip. Hence, in order to obtain this simulation result, the density of dislocation sources in the grain must be large, or at least one dislocation source must be located close enough to the stress concentration region. Intense plastic slip is then observed due to successive emission of dislocation loops on the slip plane piling up at the grain boundary. Based on these preliminary results, we

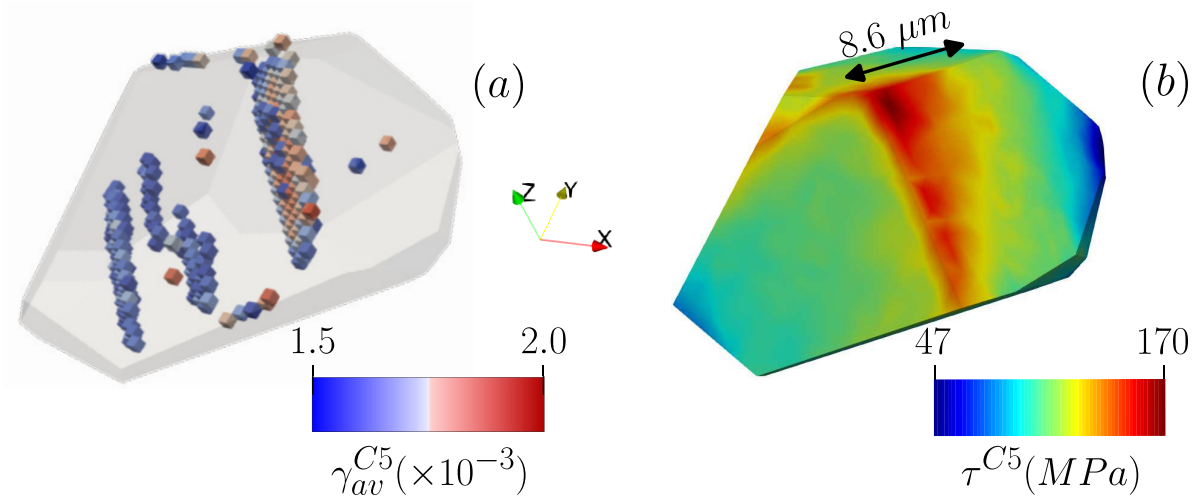

Figure 12: Local slip system activity on slip system C5 for a reduce interval ($\gamma^{C5} \in [1.5 \times 10^{-3}; 2. \times 10^{-3}]$ at the loading level of $\langle\gamma^{C5}\rangle = 0.6 \times 10^{-3}$. The most intense slip traces are shown in the grain (a) and compared with the applied stress field obtained by FEM calculation (b).

show for the first time that DDD simulations are capable of systematically reproducing and studying the elementary dislocation mechanism controlling the formation of slip bands in a polycrystal during the first stages of monotonous loading.

4.2. Contribution of dislocation cross-slip

Dislocation cross-slip is a well-known mechanism by which screw dislocations can move from their initial slip plane to a deviated plane, injecting a dislocation segment into a collinear slip system with the same Burgers vector, and possibly forming new dislocation sources. Figure 13 shows the results of two identical simulations, but one where the dislocation dynamics is solved without any contribution from the cross-slip mechanism (a) and one with the cross-slip mechanism active (b). For such simulations, the initial dislocation configuration was deliberately taken without favorable dislocation sources close to the stress concentration region. As a result, in the simulation without cross-slip illustrated in figure 13-(a) the most intense slip trace is not located near the stress concentration region but in a region where dislocation sources are available.

Examining the cross-slip simulation shown in figure 13-(b), with the same initial dislocation microstructure, we observe the emergence of a second intense slip trace formed near the stress concentration region. In the last simulation, the two intense slip traces have approximately the same intensity, of the order of half the plastic deformation concentrated in the single slip trace of the first simulation without cross-slip. This model numerical experiment illustrates the important idea that cross-slip is an essential mechanism for the spreading of plastic deformation within a grain. This propagation, associated with the apparition of new dislocation slip planes in the grain, occurs preferentially in regions of stress intensity where the formation of dislocation sources is made possible by cross-slip.

Illustration of the role of the cross-slip and double cross-slip mechanisms is well represented in figure 13 where dislocation dynamics is followed for one particular slip plane near the stress concentration region. In figure 13-(c), we show the existence of double cross-slip events associated with stress relaxation mechanism. More precisely, dislocations of the primary slip system C5 are piling up at grain boundaries thus leading to the rise of a backstress on the emitting source. Screw dislocations at equilibrium, blocked, in this pileup can eventually cross-slip [66, 75, 76], allowing plastic deformation to be accommodated. Therefore, in the small red square in figure 13-(c), cross-slip events are monitored. Segments of dislocation after a cross-slip event begin to slip on the collinear slip system B5. After a small displacement, the stress outside the pile-up configuration becomes stronger again on the primary slip system (see Table 2) and the screw sections of these bowing dislocation segments return to their original slip system C5, following the so-called double cross-slip mechanism. Exemples of such events are illustrated in figure 13-(c). Here it must be noted that such double cross-slip mechanism events do not necessarily lead to the creation of a new source and new active slip traces.

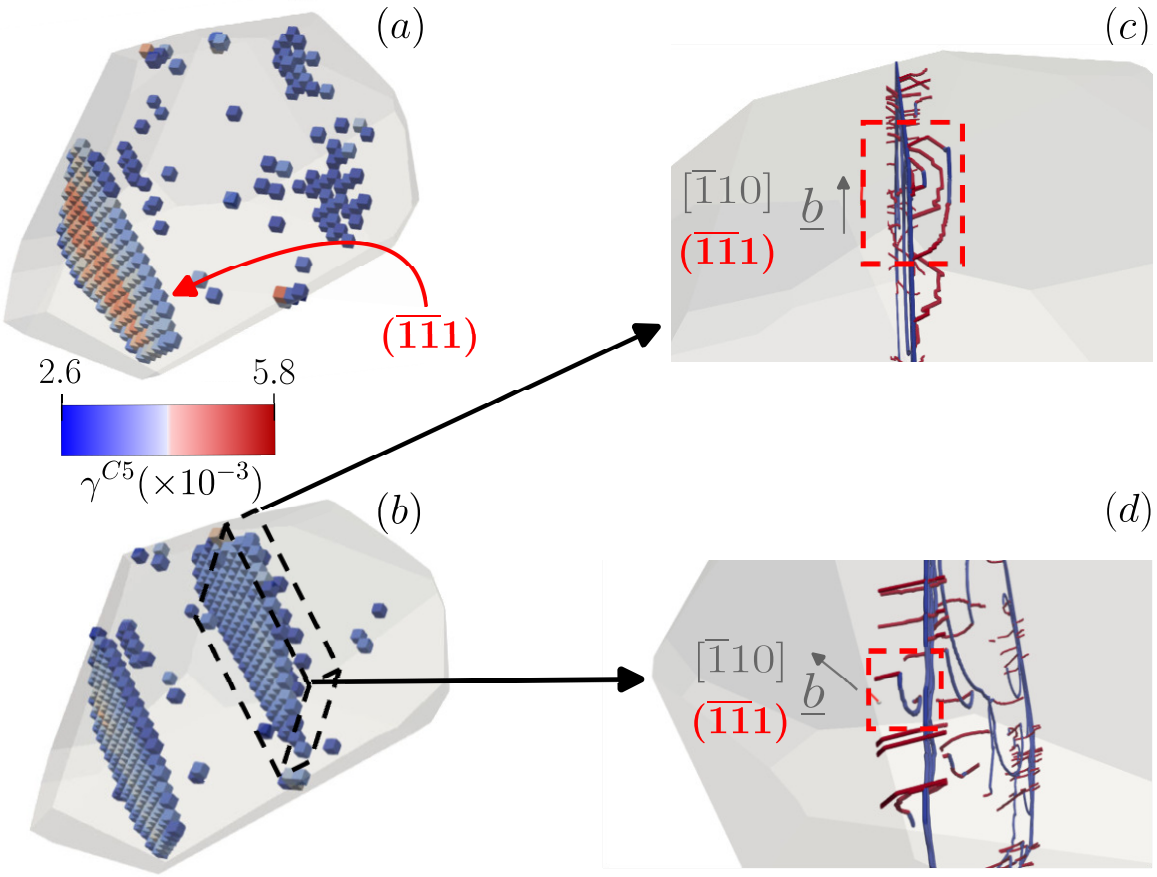

Figure 13: Illustration of the most intense regions of slip system activity associated with slip system C5 calculated over a deformation interval at the end of the simulation ($\gamma^{C5}\,[2.6 \times 10^{-3}; 5.8 \times 10^{-3}]$). Comparison between two simulations starting from the same initial dislocation configuration without cross-slip activity in (a) and with the active cross-slip mechanism in (b). (c) and (d) are further illustrations of the cross-slip activity associated with deformation near the stress concentration zone. Double cross-slip on dislocations accumulating at the grain boundary near the stress concentration zone (c). Cross-slip from other parts of the grain leading to the formation of pinning points (d). These last two observations are given by two independent slices that are not necessarily observed at the same loading level.

Indeed, many of those dislocation segments that cross-slip close to a grain boundary are blocked and can hardly evolve to become a dislocation source. Nevertheless, it was observed during the simulation that relaxation of dislocation pile-up with double-cross-slip can sometimes lead to the creation of a new source emitting many dislocations in a region of high stress.

Another dislocation source formation mechanism that we have observed is illustrated in figure 13-(d). In this second capture, the creation of a new source is monitored close to an existing slip plane C5 and through cross-slip in the central region of the grain. This cross-slip event originates from a B5 dislocation gliding in from another region of the grain and interacting elastically with the numerous dislocations of the C5 slip system accumulated in the initial slip plane C5. At the end of the process, a new C5 slip plane parallel to the one pre-existing has formed. It is important to note that for the deformation levels achieved in this type of simulation with the cross-slip, a precise comparison of the influence of the level of resolved shear stress heterogeneity on intragranular plastic slip does not reveal any major differences. For both configurations (high and low heterogeneity), it is possible to obtain more intense plastic slip in certain regions of the grain whose position varies with the applied stress field. However, the slip traces obtained in this type of comparison do not show strong differences in the intensity of plastic slip. Thus, reaching higher levels of plastic deformation is a major challenge for studying the effect of the level of heterogeneity on plastic slip.

This initial analysis of the simulation highlights the dominant role of cross-slip. As these results show, cross-slip of dislocations is a key mechanism that we should take into consideration for further investigation into the localization of intragranular plastic deformation.

5. Conclusions

In this work, the mechanisms involved in the localization of intragranular plastic strain were studied using two simulation methods, FEM and DDD. These two types of simulations were used to gain a better understanding of the phenomena of stress heterogeneity in a grain included in a polycrystalline aggregate, both on a macroscopic

scale via transgranular elastic behavior and on a mesoscopic scale via intragranular plastic behavior.

We show how the microstructure impacts the elastic loading of a grain in an aggregate leading to the heterogeneity of the stress and strain fields. Systematic computations show that the intragranular elastic loading is very dependent on interactions between grains in contact. Nevertheless, predicting the heterogeneity states of the stress inside a grain from the configuration of its neighbours is a complex problem. Systematic calculations show that the role of intersection zones is important for anticipating the creation of stress concentration zones.

A criterion based on elasticity is proposed for selecting a grain, within an aggregate, that is favorable to the localization of plastic deformation. This criterion has been statistically validated on three different configurations where the same behavior between heterogeneity and stress intensity is observed.

The criterion is used to select a polycrystalline configuration where the plasticity in a particular grain is studied using DDD simulations. These simulations show a link between the intense activity of a slip system and the stress concentration in the grain, demonstrating that polycrystalline organization is important for predicting the existence of an intragranular plastic deformation localization. The description of the simulations carried out with and without the cross-slip mechanism shows that the latter property of dislocations is a key mechanism for producing more plastic deformation near the stress concentration zone.

More systematic DDD simulations should focus on the dislocation dynamics to explain how a slip band can initiate and be persistent in a grain. A particular interest may be taken on the cross-slip and double cross-slip mechanisms. The role of heterogeneity should also be discussed with a comparison between different intragranular

elastic loading conditions identified with the proposed criterion. The criterion developed in this article is also intended to be used in conjunction with experimental observations such as Diffraction Microstructure Imaging (DMI) studies. Indeed, initial Diffraction Contrast Tomography of the specimen [77] can give access to all the grain in the cross-section and using the criterion will allow to define a hierarchy of grains to be observed in topo-tomography experiments [78, 79], which remains an important issue for future work.

In addition, particular attention should be paid to the study of grain boundary reaction mechanisms and, in particular, dislocation transmission. Indeed, in regions of stress concentrations, the loading conditions may be sufficient to allow dislocations to enter grain boundaries and possibly be transmitted to the neighbouring grain. The study of these phenomena and their role in the localization of plastic deformation would therefore be an essential part of our work. The results presented in this article being limited to elastic strain incompatibilities, it seems equally important to carry out a more detailed study using the discrete continuous model [69, 70] to study the interactions between grains during their plastic deformation. The relaxation phenomena associated with the reduction in stiffness as a result of the transition from the elastic to the plastic domain could have a significant effect on the intragranular stress state and the localization of plastic deformation. All the points detailed in this last paragraph will be the subject of specific studies which will be presented and detailed in forthcoming article(s).

Acknowledgements

This work was supported by a public grant overseen by the French National Agency (ANR) for project "3DiPolyPlast" (reference 19-CE08-0020-02).

References

[1] Ewing J A and Humfrey J 1903 *Philosophical Transactions of the Royal Society of London. Series A, Containing Papers of a Mathematical or Physical Character* **200** 241–250

[2] Crussard M C 1945 *Revue de Métallurgie* **42** 286–294

[3] Chen N and Pond R 1952 *JOM* **4** 1085–1092

[4] Brown A F 1949 *Nature* **163** 961–962

[5] Rosi F D and Mathewson C 1950 *JOM* **2** 1159–1167

[6] Ikeno S, Abou S, Tada S and Uetani Y 1990 *Journal of Japan Institute of Light Metals* **40** 918–924 ISSN 0451-5994

[7] Kitajima S and Ono N 1995 *physica status solidi (a)* **149** 201–211

[8] Konuma M 1964 *Journal of the Japan Institute of Metals* **28** 781–787

[9] Jaoul B 2008 *Etude de la plasticité et application aux métaux* (Presses des MINES)

[10] Lee T, Robertson I and Birnbaum H 1990 *Metallurgical Transactions A* **21** 2437–2447

[11] Lindholm U and Yeakley L 1965 *Journal of the Mechanics and Physics of Solids* **13** 41–53

[12] Yoshida S and Nagata N 1966 *Transactions of the Japan Institute of Metals* **7** 273–279

[13] Dimanov A, El Sabbagh A, Raphanel J, Lê T, Bornert M, Hallais S and Tanguy A 2021 *Available at SSRN 3922862*

[14] Pokharel R, Lind J, Li S F, Kenesei P, Lebensohn R A, Suter R M and Rollett A D 2015 *International Journal of Plasticity* **67** 217–234

[15] Stinville J, Ludwig W, Callahan P, Echlin M, Valle V, Pollock T and Proudhon H 2022 *Materials Characterization* **188** 111891

[16] Sangid M D, Rotella J, Naragani D, Park J S, Kenesei P and Shade P A 2020 *Acta Materialia* **201** 36–54

[17] Han S, Eisenlohr P and Crimp M A 2018 *Materials Characterization* **142** 504–514

[18] Miao J, Pollock T M and Jones J W 2012 *Acta Materialia* **60** 2840–2854

[19] Llanes L and Laird C 1992 *Materials Science and Engineering: A* **157** 21–27

[20] Stinville J, Vanderesse N, Bridier F, Bocher P and Pollock T 2015 *Acta Materialia* **98** 29–42

[21] Stinville J, Echlin M, Texier D, Bridier F, Bocher P and Pollock T 2016 *Experimental mechanics* **56** 197–216

[22] Kobayashi S, Tsurekawa S and Watanabe T 2005 *Acta Materialia* **53** 1051–1057

[23] Kobayashi S, Inomata T, Kobayashi H, Tsurekawa S and Watanabe T 2008 *Journal of materials*

science **43** 3792–3799

[24] Charpagne M, Hestroffer J, Polonsky A, Echlin M, Texier D, Valle V, Beyerlein I, Pollock T and Stinville J 2021 *Acta Materialia* **215** 117037

[25] Yeratapally S R, Glavicic M G, Hardy M and Sangid M D 2016 *Acta Materialia* **107** 152–167

[26] Stein C A, Cerrone A, Ozturk T, Lee S, Kenesei P, Tucker H, Pokharel R, Lind J, Hefferan C, Suter R M *et al.* 2014 *Current Opinion in Solid State and Materials Science* **18** 244–252

[27] Latypov M I, Stinville J C, Mayeur J R, Hestroffer J M, Pollock T M and Beyerlein I J 2021 *Scripta Materialia* **192** 78–82

[28] ANR 2023 3dipolyplast URL https://anr.fr/Project-ANR-19-CE08-0020

[29] Chen Z and Daly S 2017 *Experimental Mechanics* **57** 115–127

[30] Guo Y, Collins D, Tarleton E, Hofmann F, Tischler J, Liu W, Xu R, Wilkinson A and Britton T 2015 *Acta Materialia* **96** 229–236

[31] Roters F, Eisenlohr P, Hantcherli L, Tjahjanto D D, Bieler T R and Raabe D 2010 *Acta materialia* **58** 1152–1211

[32] Delaire F, Raphanel J and Rey C 2000 *Acta Materialia* **48** 1075–1087

[33] Zhao Z, Ramesh M, Raabe D, Cuitino A and Radovitzky R 2008 *International Journal of Plasticity* **24** 2278–2297

[34] Musienko A, Tatschl A, Schmidegg K, Kolednik O, Pippan R and Cailletaud G 2007 *Acta materialia* **55** 4121–4136

[35] Pokharel R, Lind J, Kanjarla A K, Lebensohn R A, Li S F, Kenesei P, Suter R M and Rollett A D 2014 *Annu. Rev. Condens. Matter Phys.* **5** 317–346

[36] Marano A, Gélébart L and Forest S 2019 *Acta Materialia* **175** 262–275

[37] Erinosho T and Dunne F 2015 *International Journal of Plasticity* **71** 170–194

[38] Hure J, El Shawish S, Cizelj L and Tanguy B 2016 *Journal of Nuclear Materials* **476** 231–242

[39] Barton N R, Arsenlis A and Marian J 2013 *Journal of the Mechanics and Physics of Solids* **61** 341–351

[40] Forest S 2006 *Milieux continus généralisés et matériaux hétérogènes* (Presses des MINES)

[41] Chen Y 2019 *Modélisation de la rupture ductile par approche locale: simulation robuste de la déchirure* Ph.D. thesis Paris Sciences et Lettres (ComUE)

[42] Jiang M, Fan Z, Kruch S and Devincre B 2022 *International Journal of Plasticity* **150** 103181

[43] Lepinoux J and Kubin L 1987 *Scr. Metall.;(United States)* **21**

[44] Kubin L 2013 *Dislocations, mesoscale simulations and plastic flow* vol 5 (Oxford University Press)

[45] Bulatov V and Cai W 2006 *Computer simulations of dislocations* (OUP Oxford)

[46] Hirth J P, Lothe J and Mura T 1983 *Journal of Applied Mechanics* **50** 476

[47] Jiang M 2019 *Investigation of grain size and shape effects on crystal plasticity by dislocation dynamics simulations* Ph.D. thesis Université Paris Saclay (COmUE)

[48] Madec R, Devincre B, Kubin L, Hoc T and Rodney D 2003 *Science* **301** 1879–1882

[49] Devincre B, Hoc T and Kubin L 2008 *Science* **320** 1745–1748

[50] Daveau G 2012 *Interaction dislocations-joints de grains en déformation plastique monotone: étude expérimentale et modélisations numériques* Ph.D. thesis Ecole Centrale Paris

[51] Marian J, Fitzgerald S and Po G 2020 *Handbook of Materials Modeling: Applications: Current and Emerging Materials* 2243–2271

[52] Canova G, Kubin L and Brechet Y 1993 Glide softening in alloys: a simulation *Large Plastic Deformations* ed Teodosiu C, Raphanel J and Sidoroff F (Rotterdam: A.A. Balkema) pp 27–38

[53] Meng F, Ferrié E, Déprés C and Fivel M 2021 *International Journal of Fatigue* **149** 106234

[54] Hussein A M and El-Awady J A 2016 *Journal of the Mechanics and Physics of Solids* **91** 126–144

[55] Ghoniem N, Tong S, Singh B and Sun L 2001 *Phil. Mag. A* **81** 2743–2764

[56] Ghoniem N M, Tong S H, Huang J, Singh B N and Wen M 2002 *Journal of Nuclear Materials* **307-311** 843–851

[57] Cui Y, Po G and Ghoniem N 2018 *Phys. Rev. Lett.* **120**(21) 215501

[58] Lim H, Carroll J, Battaile C C, Buchheit T, Boyce B and Weinberger C 2014 *International Journal of Plasticity* **60** 1–18

[59] Choi Y S, Groeber M A, Shade P A, Turner T J, Schuren J C, Dimiduk D M, Uchic M D and Rollett A D 2014 *Metallurgical and Materials Transactions A* **45** 6352–6359

[60] Zset 2022 http://zset-software.com/downloads/versions/ URL http://zset-software.com/downloads/versions/

[61] Quey R 2019 *no. May*

[62] Shuvalov L A, Urusovskaya A, Zheludev I, Zalessky A, Semiletov S, Grechushnikov B, Chistyakov I and Pikin S 1988 *Modern crystallography IV: physical properties of crystals* (Springer)

[63] Bretin R, Levesque M and Bocher P 2019 *International Journal of Solids and Structures* **176** 36–48

[64] Pilvin P, Onimus F, Brenner R, Pascal S, Feaugas X and Saï K 2017 *European Journal of*

Mechanics-A/Solids **61** 345–356

[65] Pourian M H, Pilvin P, Bridier F and Bocher P 2014 *Computational materials science* **92** 468–475

[66] Devincre B, Madec R, Monnet G, Queyreau S, Gatti R and Kubin L 2011 *Mechanics of Nano-objects* 81–100

[67] Van der Giessen E and Needleman A 1995 *Modelling and Simulation in Materials Science and Engineering* **3** 689

[68] Fivel M, Gosling T and Canova G 1996 *Modelling and Simulation in Materials Science and Engineering* **4** 581

[69] Vattré A, Devincre B, Feyel F, Gatti R, Groh S, Jamond O and Roos A 2014 *Journal of the Mechanics and Physics of Solids* **63** 491–505

[70] Jamond O, Gatti R, Roos A and Devincre B 2016 *International Journal of Plasticity* **80** 19–37

[71] Jiang M, Monnet G and Devincre B 2021 *Acta Materialia* **209** 116783

[72] Foreman A 1967 *Philosophical magazine* **15** 1011–1021

[73] Roy S, Gatti R, Devincre B and Mordehai D 2019 *Computational Materials Science* **162** 47–59

[74] Pearson K 1895 *proceedings of the royal society of London* **58** 240–242

[75] Brown L 2002 *Philosophical Magazine A* **82** 1691–1711

[76] Bonneville J, Escaig B and Martin J 1988 *Acta Metallurgica* **36** 1989–2002

[77] Reischig P, King A, Nervo L, Viganó N, Guilhem Y, Palenstijn W J, Batenburg K J, Preuss M and Ludwig W 2013 *Journal of Applied Crystallography* **46** 297–311

[78] Proudhon H, Guéninchault N, Forest S and Ludwig W 2018 *Materials* **11** ISSN 1996-1944

[79] Stinville J C, Ludwig W, Callahan P G, Echlin M P, Valle V, Pollock T M and Proudhon H 2022 *Material Characterization* **188** 111891 ISSN 1044-5803